Saturation Effects in a Continuous-Wave HF Chemical Laser

L. H. Sentman,* M. H. Nayfeh,† P. Renzoni,‡ K, King,§ S. Townsend,‡ and G. Tsioulos‡
University of Illinois, Urbana, Illinois

The multiline performance of a cw HF chemical laser was measured as a function of the SF_6 and H_2 flow rates, cavity losses, pressure and resonator type. The first data from a cw laser for a near-resonant energy transfer from $v=3$, $J=3,4$ to $v=2$, $J=14$ with a subsequent rotational cascade to $v=2$, $J=11$ were obtained. The stable resonator data indicated that the polarization introduced by the Brewster windows affects the power spectral distribution. The amplitude, frequency, and Fresnel number dependence of the time-dependent oscillations which were predicted to occur on lines whose saturated gain does not fill the unstable resonator were measured. The data showed that the oscillations do not occur for Fresnel numbers below 1.5 and that their amplitudes increase as the fraction of the resonator filled by the oscillating lines decreased. The a priori prediction of these characteristics of the time-dependent oscillations by the MNORO3UR computer model was in agreement with the data.

I. Introduction

In a series of studies of the performance of continuous-wave (cw) HF chemical lasers which employ confocal unstable resonators to extract power, Sentman and coworkers[1-3] employed a coupled rotational nonequilibrium kinetic fluid-dynamic wave optics code to model the laser. The results of these studies showed that rotational nonequilibrium is responsible for a time-dependent oscillation that may develop on lines whose saturated gain does not fill the resonator. For these oscillations to occur, the Fresnel number of the resonator must be greater than 1.5, the amplitude of the oscillation is determined by the fraction of the resonator that is filled by the saturated gain of the oscillating line, and the frequency of the oscillation is determined by the geometric outcoupling ratio and the fraction of the resonator that is filled by the saturated gain of the oscillating line. The objective of the present studies was to determine experimentally if the predicted time-dependent oscillations occur in the output of a cw HF chemical laser employing an unstable resonator to extract power. Because the occurrence of these time-dependent oscillations is critically dependent upon the location of the optical axis of the resonator with respect to the spatial extent of the saturated gain distribution of the lasing lines, a thorough experimental and theoretical characterization of the laser to be used in the time-dependent experiments was carried out to provide confidence in the calculation of the gain distribution of the lasing lines. The importance of this point is illustrated by a previous experiment[4] that obtained a null result (no oscillations were observed) because the saturated gain zone of the lasing lines filled the resonator.

In Sec. II, the laser performance as a function of the cavity losses and pressure is described and used to verify the computer simulations of the Helios CL II laser. The comparison of the power spectral output of the laser as a function of the cavity losses, Sec. III, indicates that a near resonant energy transfer from a high v, low J state to a low v, high J state occurs and that the power spectral distribution is affected by the polarization of the output beam. In Sec. IV, the preliminary data on the time-dependent oscillations that have been predicted to occur are presented and compared to an a priori calculation.

II. Laser Performance as a Function of Cavity Losses and Pressure

The experimental effort was directed toward characterizing the stable resonator multiline performance of the subsonic, cw, arc-driven Helios CL II laser, which has been described previously.[5] The rotational equilibrium Blaze II code[6,7] and the rotational nonequilibrium code MNORO[8] were baselined and verified with data taken with the Helios CL II laser using a 43% reflective outcoupler in vacuum mirror mounts.[5] With the outcoupler in vacuum mirror mounts, the cavity losses are known exactly since they correspond to the reflectivity of the outcoupling mirror. Vacuum mirror mount data were also taken for a 39% and 56% reflective outcoupler, and agreement between the vacuum mirror mount data and Blaze II was confirmed over a range of reflectivities.[5] It is important to note that the only input parameters to the computer models which were changed were the flow rates of SF_6 or H_2 or the mirror reflectivities. The codes correctly modeled the Helios CL II laser for various SF_6 and H_2 flow rates for a range of reflectivities.

The vacuum mirror mount data would have been sufficient if the unstable resonator to be used to measure the frequency and amplitude of the time-dependent oscillations were to be employed inside a vacuum box. In that case, the losses in the cavity would be due entirely to the mirrors and would be known. Since it is more practical to set up an unstable resonator on the Helios CL II laser using externally mounted mirrors, the additional losses introduced by the two 4-cm CaF_2 Brewster windows needed to be determined so that they could be incorporated in the codes for predicting the length of the saturated gain zones for the lasing lines. The computer codes that model the Helios CL II laser, namely, Blaze II,[6,7] MNORO,[8] and MNORO3,[9] take into account the cavity losses through the input parameter for the outcoupler reflectivity. When Brewster windows are employed, the losses they introduce in the cavity are added to the losses introduced by the outcoupling mirror, and a corresponding effective reflectivity is input into the computer codes.

Received April 24, 1984.

*Professor of Aeronautical and Astronautical Engineering. Associate Fellow AIAA.

†Associate Professor of Physics.

‡Research Assistant, Aeronautical and Astronautical Engineering. Member AIAA.

§Research Assistant, Physics.

Table 1 Comparison of Blaze II and MNORO3 results with data for the Helios CL II laser with a stable resonator with external mirror mounts and 4-cm CaF_2 Brewster windows, resulting in a 39% effective reflectivity. Primary mixing length is 0.001 cm for all cases

Run No.	32	33	34	35	36	37
$\dot{m}_{SF_6}$, g/s	1.36	1.01	0.67	1.36	1.01	0.67
$\dot{m}_{H_2}$, g/s	0.0375	0.0375	0.0375	0.0545	0.0545	0.0545
P, Torr	6.75	6.0	5.40	7.20	6.48	5.83
% SF_6 dissoc.	3.3	4.0	4.0	3.3	4.0	4.0
Initial T, K	500	450	450	500	450	450
H_2 mixing length, cm	3.0	3.5	4.0	3.0	3.5	4.0
P_T, watts						
Data	43.7	37.5	28.2	46.2	40.2	29.6
Blaze II	48.5	45.5	31.5	52.6	49.2	33.3
MNORO3		45.9	31.6		49.3	33.6
P_{10}/P_T						
Data	0.481	0.512	0.468	0.493	0.511	0.472
Blaze II	0.504	0.493	0.485	0.501	0.492	0.486
MNORO3		0.504	0.494		0.501	0.493
Beam diam, mm						
Data	4.90	5.00	5.10	4.60	4.50	4.50
Blaze II	5.30	5.60	5.70	4.10	4.30	4.30
MNORO3		5.50	5.90		4.80	4.70

Table 2 Arrangement of various optical configurations in order of decreasing effective reflectivity. Cases 7-9 used a different window from cases 10 and 11

Case No.	Effective reflectivity, %	Optical configuration[a]
1	56	56% reflective outcoupler and ETR in VMM
2	43	43% reflective outcoupler and ETR in VMM
3	41	56% reflective outcoupler in EMM, ETR in VMM, left-hand 4-cm CaF_2 BW
4	39	56% reflective outcoupler and ETR in EMM, two 4-cm CaF_2 BW
5	39	39% reflective outcoupler and ETR in VMM
6	23	39% reflective outcoupler and ETR in EMM, two 4-cm CaF_2 BW
7	22	56% reflective outcoupler in EMM, ETR in VMM, left-hand 1-in. CaF_2 BW, case A, window 2
8	22	56% reflective outcoupler in EMM, ETR in VMM, left-hand 1-in. CaF_2 BW, case B, window 2
9	15	56% reflective outcoupler in EMM, ETR in VMM, left-hand 1-in. CaF_2 NBW, case C, window 2
10	9	56% reflective outcoupler in EMM, ETR in VMM, left-hand 1-in. CaF_2 BW, case A, window 1
11	8	56% reflective outcoupler in EMM, ETR in VMM, left-hand 1-in. CaF_2 BW, case B, window 1

[a]VMM denotes vacuum mirror mounts; EMM, external mirror mounts; ETR enhanced total reflector; BW Brewster windows; NBW non-Brewster window.

For the x_c of the peak power for each stable resonator optical configuration, total power, beam diameter, pressure distribution, and power spectral distribution were measured for fixed He and O_2 flow rates for the six SF_6 and H_2 flow rate combinations used previously.[2,5] The total multiline power was measured by placing a power meter in front of the outcoupled beam after the beam had gone through a 10% chopper. The power spectral distribution was measured using a scanning monochromator and a PbSe detector, whose output was recorded on a strip chart recorder (Fig. 1). The power spectral distributions were obtained by measuring the relative heights of the signal for each line on the strip chart trace. The wavelength of each line was determined from a wavelength-dependent signal from the monochromator scanning motor which was recorded on the second channel of the strip chart recorder. The spectra are the average of a minimum of two scans for each run. For all runs, one burn block was taken 34.3 cm from the outcoupling mirror and one burn block was taken 5 cm from the outcoupling mirror. The beam diameter at the outcoupling mirror was extrapolated for all runs using the beam divergence determined from the two burn blocks. The pressure distribution was measured with a mercury manometer bank. The manometer bank is connected to 10 pressure taps along the channel centerline and to 10 off-centerline pressure taps in each laser body. The static pressure was thus determined for the entire flowfield through the laser body. Whenever externally mounted mirrors and Brewster windows were used, the intracavity beam path was purged with N_2. The vacuum mirror mounts and the Brewster windows were purged with He. When externally mounted mirrors and Brewster windows were employed, the entire optical cavity was rigidly attached to an invar rod structure mounted on two translation stages. Once the mirrors were aligned, the location of the optical axis was determined by the translation stages.

When vacuum mirror mounts were employed, a parallel plate polarization analyzer showed that the laser output beam was randomly polarized, i.e., the power in all orientations of the polarization vector was the same. When Brewster windows with externally mounted mirrors were employed, the laser output beam was polarized with approximately 84% of the power in the orientation corresponding to minimum loss going through the Brewster windows and with 16% of the power in the orientation which is perpendicular to the minimum loss orientation. Thus, the Brewster windows introduced losses into the optical cavity.

The losses introduced by the two 4-cm CaF_2 Brewster windows were determined by a direct measurement and by an indirect measurement. In the direct measurement, the Brewster windows were placed in the path of the output beam, and the losses were determined from the difference in the multiline power of the output beam before and after going through the Brewster windows. These measurements were taken outside the optical cavity for an unpolarized output beam and for a polarized output beam. In an effort to simulate the losses introduced by the Brewster windows when they are employed on the laser, the losses were measured by putting the Brewster windows inside the optical cavity. The direct measurement of the losses introduced by the Brewster windows did not give consistent results and, thus, an indirect measurement of the losses was used.

The indirect measurement was accomplished by mounting the Brewster windows on the laser and measuring the total power for the six combinations of SF_6 and H_2 flow rates. Total powers were measured for the 56% and 39% reflective outcouplers with the two 4-cm CaF_2 Brewster windows and for the 56% reflective outcoupler with the left-hand 4-cm Brewster window and the enhanced total reflector in a vacuum mirror mount. To find an average effective reflectivity for the two Brewster window configurations, the Brewster window data for the 56% reflective outcoupler were placed on the P_T vs reflectivity curves generated by Blaze II and the vacuum mirror mount data (Fig. 2). Taking the average of the effective reflectivities for the six flow rates gave an average effective reflectivity of 41% for the 56% reflective outcoupler with the left-hand 4-cm Brewster window and 39% for the 56% reflective outcoupler with the two

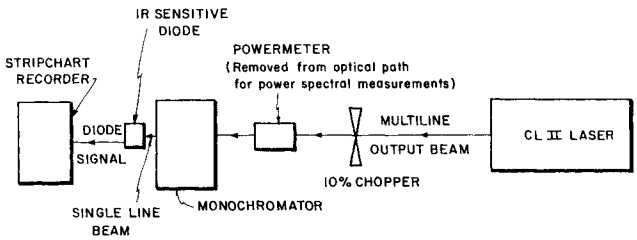

Fig. 1 Block diagram of the setup for power and power spectral measurements for the Helios CL II laser. For the power spectral measurements, the power meter is removed from the optical path.

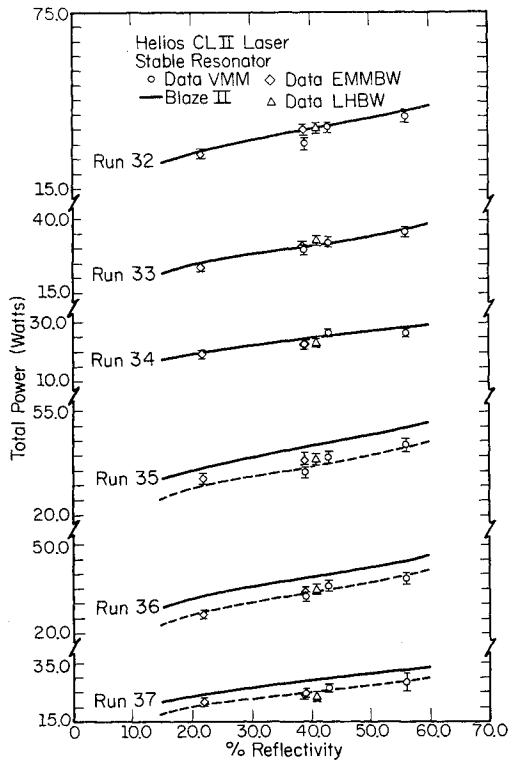

Fig. 2 Comparison of experimental and predicted laser performance vs mirror reflectivity for Helios CL II laser when 4-cm Brewster windows are used with the 56% and the 39% reflective outcouplers. VMM denotes vacuum mirror mount; EMMBW, external mirror mounts with two Brewster windows; LHBW, external mirror mount with left-hand Brewster window. Dashed lines are curves drawn through the data points.

4-cm Brewster windows. This gives an effective loss of 15% for the left-hand 4-cm Brewster window and 17% for the two 4-cm Brewster windows. The 2% difference in losses from one Brewster window to two Brewster windows can be explained by the fact that in the two Brewster windows case, the first Brewster window polarizes the beam and, therefore, the polarized beam has minimal losses going through the second Brewster window. From Fig. 2 it is seen that when the average effective reflectivities are used, the Brewster window data fall on the previously determined P_T vs reflectivity curves for all six flow rates. Clearly, for this procedure to be valid, the losses introduced in the cavity by two Brewster windows should be the same when they are used with the 56% and 39% reflective outcouplers. When the average loss of 17% for the two 4-cm Brewster windows is subtracted from the 39% reflectivity of the outcoupler, the effective reflectivity is 22%. When the total powers for the 39% reflective outcoupler are plotted on the P_T vs reflectivity curves using the effective reflectivity of 22%, the data fall on

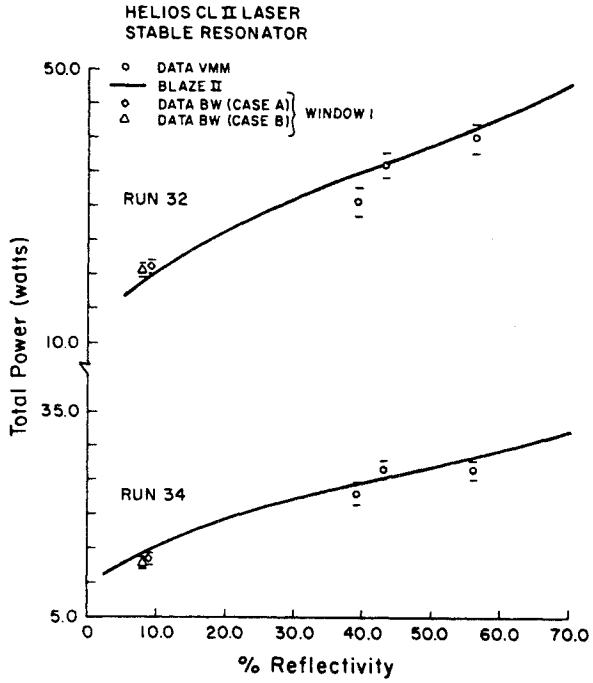

Fig. 3 Comparison of experimental and predicted laser performance vs mirror reflectivity for the Helios CL II laser when window 1 in a 1-in. Brewster window mount is used with the 56% reflective outcoupler for two orientations, case A and case B. VMM denotes vacuum mirror mount; BW, external mirror mount with 1-in. Brewster window.

these curves (Fig. 2). Thus, the Brewster window losses determined from the indirect measurement are correct.

Using the 4-cm Brewster windows limited the range of effective reflectivities that could be considered to above 20%. The 1-in. Brewster windows, which could also be used on the laser, were known to introduce more losses into the cavity than the 4-cm Brewster windows, and their exact losses were determined by the indirect measurement method. Not only did the 1-in. Brewster windows allow the range of the data to go to lower effective reflectivities of the outcoupler but, unlike the 4-cm Brewster windows, they could also be rotated to determine the effect of rotating the polarization vector on the Brewster window losses. The losses introduced in the cavity by a 1-in. non-Brewster window were also investigated. Total powers and power spectral distributions were taken for two 1-in. windows for runs 32 and 34. The effective reflectivities determined from the total powers and the experimental P_T vs reflectivity curves are summarized in Fig. 3 for one of the windows. For the first window, the average effective reflectivities are 9% and 8% for cases A (polarization vector perpendicular to the flow) and B (polarization vector parallel to the flow), respectively. For the second window, the average effective reflectivity is 22% for both cases A and B, and 15% for case C (window perpendicular to optical axis). For both windows, the effective reflectivity is nearly the same in case A as in case B, thus showing that rotating the polarization vector does not affect the losses introduced by a Brewster window.

In addition to varying the optical cavity losses for a fixed flow rate, the pressure in the lasing zone was varied from 5 to 15 Torr by changing the size of the opening in the flow control valve, which was upstream of the vacuum pump. Since the longest saturated gain zones occur at the lowest pressures, stable resonator data were obtained as a function of x_c for the six SF_6 and H_2 flow-rate combinations with the flow-control valve wide open. For the x_c of peak power, beam diameters, pressure, and spectra were measured. These data were taken with the 56% mirror and two 4-cm CaF_2

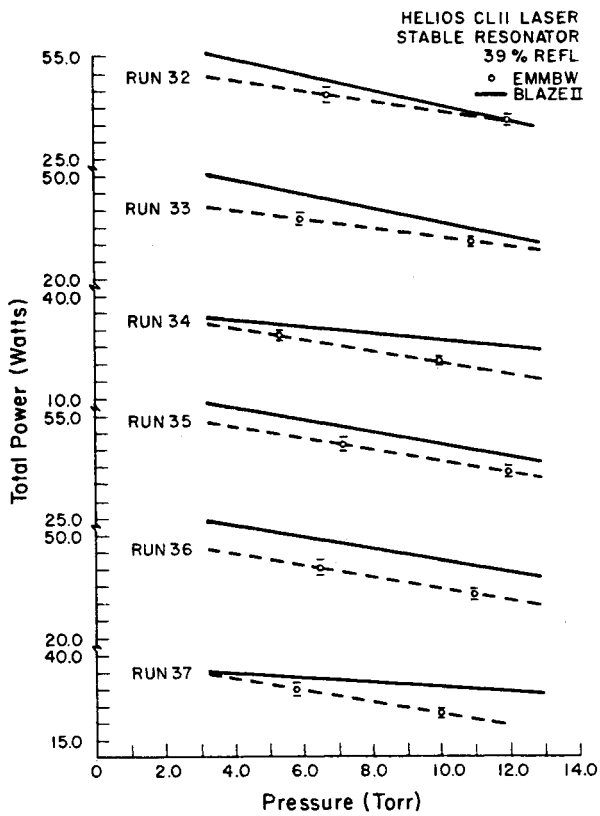

Fig. 4 Comparison of experimental and predicted laser performance vs pressure for the Helios CL II laser when Brewster windows are used with the 56% reflective outcoupler. EMMBW denotes external mirror mounts with two Brewster windows; the effective cavity reflectivity was 39%. Dashed lines are drawn through the data points.

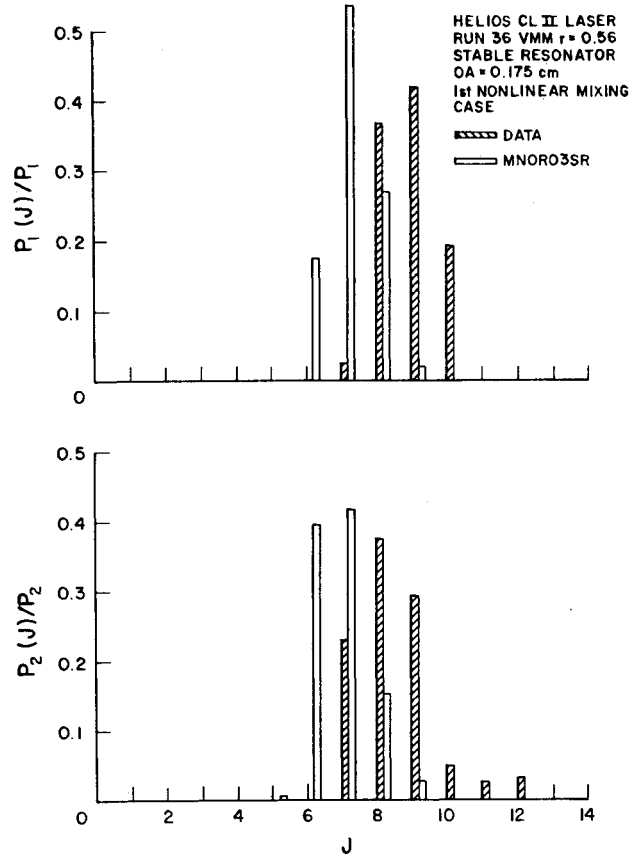

Fig. 5 Experimental and MNORO3SR power spectral distributions for the Helios CL II laser for run 36 for vacuum mirror mounts, $r=0.56$, $p=11$ Torr.

Brewster windows, which corresponds to an effective reflectivity of 39%. In Fig. 4 the Blaze II computer model is compared to the data as a function of cavity pressure. The only parameter changed in the model for these calculations was the initial pressure at the inlet to the laser cavity. From Fig. 4 it is seen that the model gives very good agreement with the data over the entire pressure range accessible with our vacuum system. Thus, the model agrees with the data as flow rates, cavity losses, and pressure are varied. This provides confidence in the model's prediction of the lengths of the saturated gain zones of the lasing lines.

The low pressure data at the x_c for peak power are summarized in Table 1. Since the run 34 flow rates gave the largest beam diameter, the unstable resonator experiments were performed for this flow rate.

III. Media Saturation and Polarization Effects on the Laser Power Spectral Distribution

In the preceding section, the total power of the laser as a function of the optical cavity losses and pressure was presented. In this section, the effect of the optical configuration on the power spectral distribution of the laser will be examined. All of the data presented in this section are for the high cavity pressures of 10-12 Torr for the stable resonator. To facilitate discussion of the performance of the laser as a function of the various optical configurations, they are listed in order of decreasing effective reflectivity in Table 2. The total power, fraction of the power in the $1\rightarrow0$ vibrational band, beam diameter, and power spectral distribution for these cases are presented in Tables 3-8 for the six combinations of SF_6 and H_2 flow rates.

Comparison of the power spectral distributions of cases 1 and 2 shows that as the cavity losses decrease, the power spectral distribution shifts toward higher J's. It is evident that more lines are present with the 56% reflective outcoupler than with the 43% reflective outcoupler. The additional lines $P_1(10)$, $P_1(12)$, and $P_2(10)$ to $P_2(12)$ are the result of the lower losses associated with the higher outcoupler reflectivity, which permits lines with smaller gains to lase. Two unexpected results were the presence of $P_1(10)$ and $P_1(12)$, with the absence of $P_1(11)$ for the high SF_6 flow rate for both H_2 flow rates, and the presence of $P_2(10)$ to $P_2(12)$, with a minimum at $P_2(11)$ for the middle and high SF_6 flow rates for both H_2 flow rates. Since the lines $P_1(10)$, $P_1(12)$ and $P_2(10)$-$P_2(12)$ are not predicted by MNORO3, which employs a Fabry-Perot resonator, these cases were studied with a stable resonator model to determine to what extent the occurrence of these lines and the minima at $P_1(11)$ and $P_2(11)$ are a consequence of the upstream-downstream coupling of the stable resonator.[3] From Fig. 5, it is seen that the extra lines that lase in the Fabry-Perot model do not lase in the stable resonator model MNORO3SR[3] and the power spectral distribution is in much better agreement with the data. The results of this study indicated that the minima in the power spectral distribution at $P_1(11)$ and $P_2(11)$ are not a consequence of the type of resonator used.

An examination of the energy-level diagram for HF, Fig. 6, indicates a near resonance between the levels $v=3$, $J=3,4$ and $v=2$, $J=14$ and the levels $v=2$, $J=3,4$ and $v=1$, $J=14$. The minimum in the spectra at $P_2(11)$ may be evidence for a kinetic effect, namely, a near resonant transfer from $v=3$, $J=3,4$ to $v=2$, $J=14$ with a subsequent rotational cascade to $v=2$, $J=11$, which is the upper level for the $P_2(12)$ line. Since $P_2(12)$ lases, the rotational cascade to $v=2$, $J=10$, which is the upper level for the $P_2(11)$ line, is blocked, resulting in $P_2(11)$ being weaker than $P_2(12)$. Similarly, a near resonant transfer may occur from $v=2$, $J=3,4$ to $v=1$,

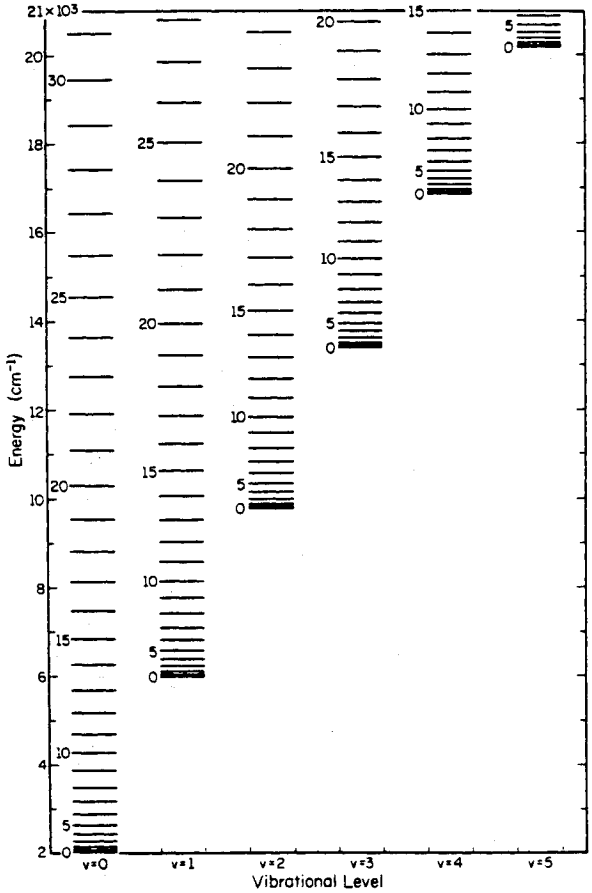

Fig. 6 HF energy-level diagram.

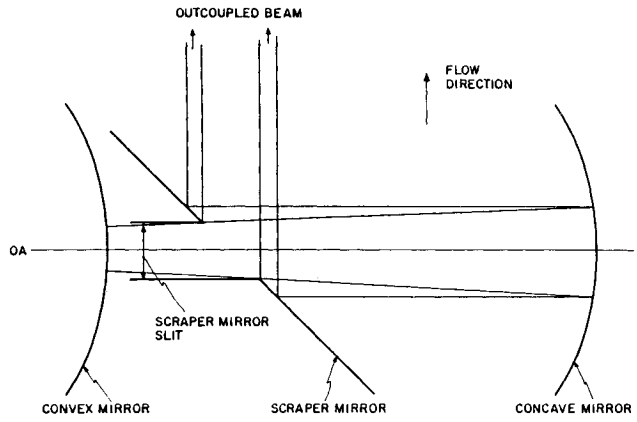

Fig. 7 Layout of the unstable resonator used in the measurement of the time-dependent oscillations on lines whose saturated gain does not fill the resonator. The resonator was aligned with the upstream edge at the H_2 injectors. Each half of the slit scraper mirror was independently adjustable with a micrometer.

$J=14$ with a subsequent rotational cascade to $v=1$, $J=11$, which is the upper level for the $P_1(12)$ line. Since $P_1(12)$ lases, the rotational cascade to $v=1$, $J=10$, which is the upper level for the $P_1(11)$ line, is blocked resulting in $P_1(11)$ being weaker than $P_1(12)$.

Comparison of cases 3, 4, and 6 shows that the power spectral distribution shifted toward higher J's as the cavity losses decreased and as the H_2 and/or SF_6 flow rates increased. Cases 3, 4, and 6 introduced polarization into the cavity through the Brewster windows but the difference in performance between these three cases is due entirely to the differences in cavity losses. Clearly, the performance of the vacuum mirror mount cases[5] and the Brewster window cases are affected in the same way by changes in cavity losses and by changes in the H_2 and SF_6 flow rates. Polarization does not alter the behavior of the laser as the cavity losses or the flow rates are varied.

Cases 7-11 also employed a Brewster window, but instead of using the 4-cm CaF_2 Brewster windows used in the other Brewster window cases, they used a 1-in. CaF_2 Brewster window. Cases 7-9 and cases 10 and 11 used two different windows. In Sec. II, it was shown that changing the orientation of the polarization vector did not affect the losses introduced by the Brewster window. Consequently the power spectral distributions for cases using different orientations of the polarization vector but the same window are similar (see Tables 3 and 5). Cases 7 and 8 show that changing the orientation of the polarization vector does not affect the minimum at $P_2(11)$. In case 7 the minimum is at $P_2(10)$, while in case 8 it is at $P_2(11)$. This discrepancy is due to the error associated with taking the power spectral distributions, especially when the lines are weak. What is significant is that $P_2(10)$ in case 7 and $P_2(11)$ in case 8 are less than $P_2(12)$.

Case 6 and cases 7 and 8 employ different Brewster windows but have nearly the same effective reflectivity. In Table 3 it can be seen that the power spectral distributions for case 6 and for cases 7 and 8 are drastically different. A detailed understanding of the occurrence of $P_1(10)$ and of $P_2(10)$-$P_2(12)$, with a minimum at $P_2(10)$ in case 7 and at $P_2(11)$ in case 8, is lacking at present. The difference in the power spectral distributions may be due to some difference between the 4-cm CaF_2 windows and the 1-in. CaF_2 window. Also, the difference in how the helium purge flow enters the laser through the two 4-cm CaF_2 Brewster windows and how it enters the laser through the 1-in. CaF_2 Brewster window may contribute to the occurrence of the additional lines in cases 7 and 8.

The power spectral distribution of cases that include Brewster windows shifts toward higher J's as the cavity losses are reduced and as the SF_6 and/or H_2 flow rate is increased. The cases that employ vacuum mirror mounts behave similarly as a function of H_2 and SF_6 flow rates and as a function of outcoupler reflectivity. The shift of the spectra toward higher J's as the SF_6 or H_2 flow rates increase is a consequence of the increase in temperature which results from the increased production of HF as these flow rates increase. In Tables 3 to 8, the power spectral distributions are tabulated for all the cases in order of decreasing effective reflectivity, and it is clearly evident that the shift of the power spectral distribution toward higher J's with increasing effective reflectivity applies only to cases employing vacuum mirror mounts or to cases employing Brewster windows but not to a combination of the two types of cases.

The differences in the performance of cases employing vacuum mirror mounts and cases employing Brewster windows become apparent by comparing case 2 to cases 3 and 4. The total losses in cases 3 and 4 are only 2 to 5% less than in case 2, yet the power spectral distributions in cases 3 and 4 contain the lines $P_2(10)$-$P_2(12)$ at the middle and high SF_6 flow rates, which are not seen in case 2. The lines $P_2(10)$-$P_2(12)$, with a minimum at $P_2(11)$, which appeared in case 1, were attributed to the lower losses associated with the 56% reflective outcoupler compared with the 43% reflective outcoupler of case 2. When the losses associated with the Brewster window cases are large enough, as in case 6, these lines do not appear. These comparisons suggest that the polarization of the laser introduced by the Brewster windows plays a role in the occurrence of these lines in cases 3 and 4. At the middle and high SF_6 flow rates, runs 32, 33, 35, and 36, the polarization also promotes the appearance of $P_1(10)$, and it appears to suppress lines $P_1(6)$ and $P_2(6)$. A weaker polarization effect is seen in the low SF_6 flow-rate cases,

Table 3 Comparison of experimental data for flow rates of run 32 for various combinations of mirrors and Brewster windows

Case No.	r_{effect}	P_T, W	P_{10}/P_T	Beam diam, mm
1	56%	39.5	0.522	3.57
2	43%	35.0	0.475	2.92
3	41%	36.0	0.508	3.27
4	39%	35.5	0.530	3.39
5	39%	32.5		
6	23%	27.0-28.0	0.507	
7	22%	28.25	0.508	
8	22%	29.25	0.512	
9	15%	26.5	0.503	
10	9%	21.0		
11	8%	20.5		

	$P_v(J)/P_T$											
Case No.	$P_1(6)$	$P_1(7)$	$P_1(8)$	$P_1(9)$	$P_1(10)$	$P_1(12)$	$P_2(6)$	$P_2(7)$	$P_2(8)$	$P_2(9)$	$P_2(10)$	$P_2(11)$	$P_2(12)$
1		0.0122	0.1940	0.2358	0.0783	0.0013		0.0761	0.1946	0.1563	0.0174	0.0071	0.0267
2		0.1917	0.1912	0.0925			0.1340	0.2034	0.1645	0.0227			
3		0.0764	0.1728	0.1645	0.0943			0.1448	0.1677	0.1394	0.0173	0.0051	0.0177
4		0.0515	0.1968	0.2064	0.0752			0.1441	0.1865	0.1068	0.0057	0.0045	0.0225
5					No spectra were taken								
6		0.1597	0.2860	0.0616			0.0263	0.2712	0.1894	0.0058			
7		0.0540	0.2573	0.1660	0.0304			0.1837	0.2451	0.0569	0.0010	0.0022	0.0034
8		0.0495	0.1973	0.1646	0.1009			0.1460	0.1926	0.1242	0.0020	0.0016	0.0213
9		0.0033	0.2349	0.1994	0.0652			0.1772	0.2219	0.0900			0.0081
10					No spectra were taken								
11					No spectra were taken								

Table 4 Comparison of experimental data for flow rates of run 33 for various combinations of mirrors and Brewster windows

Case No.	r_{effect}	P_T, W	P_{10}/P_T	Beam diam, mm
1	56%	36.5	0.504	4.30
2	43%	32.5	0.477	3.03
3	41%	32.5	0.534	3.49
4	39%	30.5	0.483	3.43
5	39%	30.5		
6	23%	23.5	0.528	

	$P_v(J)/P_T$											
Case No.	$P_1(6)$	$P_1(7)$	$P_1(8)$	$P_1(9)$	$P_1(10)$	$P_2(6)$	$P_2(7)$	$P_2(8)$	$P_2(9)$	$P_2(10)$	$P_2(11)$	$P_2(12)$
1		0.0594	0.2086	0.1764	0.0594		0.1440	0.2145	0.1192	0.0094	0.0029	0.0062
2	0.0429	0.2073	0.1778	0.0509		0.1693	0.2324	0.1230				
3		0.1401	0.1776	0.1680	0.0480	0.0054	0.1754	0.1714	0.1112	0.0018		0.0011
4		0.1393	0.2165	0.1253	0.0019	0.0338	0.1995	0.2038	0.0799			
5					No spectra were taken							
6		0.2051	0.2436	0.0793		0.0584	0.2172	0.1941	0.0023			

runs 34 and 37. In these cases, the polarization appears to promote the occurrence of lines $P_1(9)$ and $P_2(9)$.

The polarization effect is more pronounced at higher SF_6 flow rates, but for all six combinations of SF_6 and H_2 flow rates, it causes the power spectral distribution to shift toward higher J's. When lines $P_2(10)$-$P_2(12)$ appear in cases 3 and 4, the minimum occurs at $P_2(11)$. This indicates that polarization does not affect the minimum at $P_2(11)$ and that the minimum in the spectra may be the result of the kinetic effect described previously.

IV. Time-Dependent Oscillations in an Unstable Resonator

With the confidence provided by the computer model's agreement with the data for the Helios CL II laser as the flow rates, cavity losses, and pressure were varied, a series of calculations were performed with the MNORO3 rotational nonequilibrium model coupled to a strip resonator, wave optics model of an unstable resonator (denoted MNORO3UR).[3] Since the MNORO3UR calculations[3] indicated that the occurrence of the time-dependent oscillations on lines whose saturated gain does not fill the unstable resonator is Fresnel number-dependent, the experiments were performed for the flow conditions that gave the longest saturated gain regions. These occurred for the low SF_6 and low H_2 flow rates of run 34 with the flow-control valve wide open, which gave a laser cavity pressure of 5.3 Torr. Since the resonator used in the experiments was a 50% geometric outcoupled, symmetric, confocal unstable resonator, the effective size of the concave mirror was twice the size of the hole in the scraper mirror. Because the Fresnel number[¶] of the resonator is determined by the size of the concave mir-

[¶]Fresnel number $N_F = D^2/4\,\lambda L$ where D is the diameter of the concave mirror, λ is the wavelength, and L is the mirror spacing.

Table 5 Comparison of experimental data for flow rates of run 34 for various combinations of mirrors and Brewster windows

Case No.	r_{effect}	P_T, W	P_{10}/P_T	Beam diam, mm
1	56%	27.5	0.468	3.06
2	43%	26.0	0.495	2.89
3	41%	24.0	0.483	3.35
4	39%	20.5-20.75	0.472	2.91
5	39%	24.0		
6	23%	19.5-19.75	0.460	
7	22%	19.25		
8	22%	18.5		
9	15%	15.5		
10	9%	13.75	0.483	
11	8%	13.5	0.439	

	$P_v(J)/P_T$										
Case No.	$P_1(6)$	$P_1(7)$	$P_1(8)$	$P_1(9)$	$P_1(10)$	$P_2(6)$	$P_2(7)$	$P_2(8)$	$P_2(9)$	$P_2(10)$	$P_2(11)$	$P_2(12)$
1	0.0010	0.1703	0.1969	0.0997		0.0979	0.1903	0.1593	0.0848			
2	0.1237	0.2139	0.1578			0.2030	0.1963	0.1056				
3	0.0164	0.1904	0.1827	0.0935		0.1356	0.1787	0.1508	0.1519			
4	0.0315	0.1974	0.1868	0.0558		0.1240	0.2491	0.1287	0.0267			
5					No spectra were taken							
6	0.0151	0.2848	0.1596			0.2318	0.2132	0.0955				
7					No spectra were taken							
8					No spectra were taken							
9					No spectra were taken							
10	0.0587	0.2893	0.1351			0.1939	0.2225	0.0914	0.0091			
11	0.0076	0.2639	0.1676			0.1667	0.2719	0.1198	0.0024			

Table 6 Comparison of experimental data for flow rates of run 35 for various combinations of mirrors and Brewster windows

Case No.	r_{effect}	P_T, W	P_{10}/P_T	Beam diam, mm
1	56%	43.0	0.503	2.98
2	43%	39.0	0.491	2.84
3	41%	39.0	0.497	2.99
4	39%	38.0	0.520	3.21
5	39%	35.5		
6	23%	31.5	0.553	

	$P_v(J)/P_T$												
Case No.	$P_1(6)$	$P_1(7)$	$P_1(8)$	$P_1(9)$	$P_1(10)$	$P_1(12)$	$P_2(6)$	$P_2(7)$	$P_2(8)$	$P_2(9)$	$P_2(10)$	$P_2(11)$	$P_2(12)$
1		0.0241	0.1466	0.1962	0.1225	0.0138		0.0607	0.1979	0.1333	0.0484	0.0149	0.0416
2		0.1614	0.2021	0.1276			0.0897	0.1834	0.1739	0.0617			
3		0.0731	0.1888	0.1637	0.0717			0.1671	0.1852	0.1234	0.0062	0.0069	0.0139
4		0.0498	0.2107	0.1753	0.0844			0.1350	0.1957	0.1163	0.0115	0.0046	0.0167
5					No spectra were taken								
6		0.1121	0.2681	0.1729				0.1811	0.2136	0.0522			

ror, the Fresnel number of the resonator was varied by designing the scraper mirror so that the slit width could be varied from 0 to 1 cm. Because the resonator was always aligned with the upstream edge at the H_2 injectors and the resonator was symmetric, the distance between the optical axis and the H_2 injectors was equal to the slit width. The concave, convex, and scraper mirrors were attached to a rigid invar rod structure mounted on two translation stages. Once the resonator was aligned, the optical axis location was set by moving the translation stages. The layout of the unstable resonator is shown in Fig. 7.

The measurements were made using a room temperature InAs detector which had a 2-ns rise time (determined by measuring a 10-ns pulse from a Nd-Yag laser). The output beam was chopped with a mechanical chopper. The entire beam was allowed to impinge on the detector to measure the oscillations of the total power. To measure the oscillations on individual lines, the output beam was first passed through a constant efficiency spectrometer,[10] which allowed the output of one line at a time to impinge on the detector. To obtain the period of the oscillations, the output of the detector was displayed on a 500-MHz oscilloscope. To determine the time dependence of the frequency of the oscillations, the signal was also displayed on a 40-MHz spectrum analyzer. Since the 500-MHz scope only displayed the ac part of the signal, to obtain the amplitude modulation, the signal was displayed on a 100-MHz scope.

The data for the total power for the low SF_6 and H_2 flow rates are shown as a function of Fresnel number in Table 9. The line denoted MNORO3UR is the result of a calculation using the coupled rotational nonequilibrium-wave optics model of our laser.[3] This calculation was performed before the experiments to determine whether the oscillations should occur when the optical axis is 5 mm downstream of the H_2 injectors. All of the calculations indicated that the period should be 40 ns, independent of the Fresnel number.[3] From Table 9, it is seen that in addition to the expected 40-ns oscillation, there was a 7-ns oscillation superimposed on top of it. Since the mirror spacing of the resonator was 1 m and the round-trip transit time is 6.67 ns, the 7-ns oscillation

Table 7 Comparison of experimental data for flow rates of run 36 for various combinations of mirrors and Brewster windows

Case No.	r_{effect}	P_T, W	P_{10}/P_T	Beam diam, mm
1	56%	37.5	0.461	2.83
2	43%	36.0	0.471	2.86
3	41%	34.5	0.503	3.06
4	39%	32.5	0.531	3.06
5	39%	32.0-33.0		
6	23%	25.5	0.548	

	$P_v(J)/P_T$										
Case No.	$P_1(6)$	$P_1(7)$	$P_1(8)$	$P_1(9)$	$P_1(10)$	$P_2(6)$	$P_2(7)$	$P_2(8)$	$P_2(9)$	$P_2(10)$	$P_2(11)$	$P_2(12)$
1		0.0108	0.1684	0.1929	0.0886		0.1240	0.2019	0.1574	0.0270	0.0129	0.0161
2	0.0237	0.1778	0.1987	0.0709		0.1410	0.1964	0.1652	0.0261			
3		0.0321	0.1699	0.1966	0.1039		0.0826	0.2005	0.1467	0.0327	0.0113	0.0237
4		0.0995	0.2270	0.1647	0.0393	0.0007	0.1893	0.1835	0.0919	0.0027	0.0008	0.0006
5					No spectra were taken							
6		0.1118	0.2665	0.1700		0.0007	0.1836	0.2219	0.0455			

Table 8 Comparison of experimental data for flow rates of run 37 for various combinations of mirrors and Brewster windows

Case No.	r_{effect}	P_T, W	P_{10}/P_T	Beam diam, mm
1	56%	31.5	0.482	2.32
2	43%	26.0	0.495	2.77
3	41%	24.0	0.495	2.81
4	39%	22.0-22.25	0.474	3.09
5	39%	25.0		
6	23%	21.5	0.464	

	$P_v(J)/P_T$										
Case No.	$P_1(6)$	$P_1(7)$	$P_1(8)$	$P_1(9)$	$P_1(10)$	$P_2(6)$	$P_2(7)$	$P_2(8)$	$P_2(9)$	$P_2(10)$	$P_2(11)$	$P_2(12)$
1	0.0193	0.1842	0.1949	0.0836		0.1494	0.1885	0.1231	0.0572			
2	0.1292	0.2152	0.1510			0.1913	0.1932	0.1201				
3		0.1701	0.1806	0.1439		0.1028	0.1736	0.1589	0.0701			
4	0.0090	0.2208	0.1776	0.0662		0.1286	0.2022	0.1594	0.0362			
5					No spectra were taken							
6	0.0047	0.2837	0.1755			0.2040	0.2165	0.1156				

probably corresponds to a mode beating. Table 9 shows that the time-dependent oscillations on lines whose saturated gain does not fill the resonator do not occur for Fresnel numbers below 1.5 and that their amplitudes increase as the fraction of the resonator filled by the oscillating lines decreases.

Table 10 gives the data for individual lines for the 3- and 4-mm slit widths. It should be noted that there is a strong cascade coupling between the oscillating $1\rightarrow0$ and $2\rightarrow1$ lines, that is, if $P_2(6)$ oscillates, then $P_1(7)$ also oscillates. From a comparison of the 3- and 4-mm slit cases, it is generally seen that as the fraction of the resonator filled by a line decreases, the amplitude of its oscillation increases.

To provide a qualitative comparison, the theoretical calculations for the 5-mm slit case are shown with the 4-mm slit data. The 5-mm slit calculation is qualitative because the losses introduced by the Brewster windows were not included. In the future, a calculation that includes the effect of the Brewster windows will be performed for the 4-mm slit case. It is seen that there is qualitative agreement between the calculation and the data. The difference in lasing lines between the calculations and the data is due to the omission in the calculation of the losses introduced by the Brewster windows.

To verify experimentally that oscillations on lines whose saturated gain does not fill the unstable resonator do not occur from Fresnel numbers less than 1.5, the x_c of the optical axis was varied from 2 mm to 4 mm for the scraper mirror slit width of 2 mm (Fresnel number of 1.428). No 40-ns oscillations were observed for any optical axis location. The 7-ns oscillation was observed on some lines.

Table 9 Frequency and amplitude of time-dependent oscillation of total power as function of Fresnel number for flow rates of run 34 at 5.3 Torr

Run 34, symmetric confocal unstable resonator					
Scraper mirror slit, mm	N_F	P_{CAV} Torr	P_T Watts	OSC period ns	Amplitude modulation $\%P_T$
1.0	0.357	5.31	7.25	7	
2.0	1.428	5.30	11.7	7	
3.0	3.214	5.29	9.5	40/7	3.0
4.0	5.714	5.31	7.0	40/7	22.0
5.0	8.929	5.34	2.25	40/7	25.0
MNORO3UR[a]				40	36.0
6.0	12.857	5.31	0.98	40	50.0

[a]MNORO3UR is the result of a calculation performed before measurements were made to determine if time-dependent oscillations should occur when optical axis is 5 mm downstream of H_2 injectors.

From the comparison of the calculation with the data, it is seen that the predicted variations of the time-dependent oscillations on lines whose saturated gain does not fill the resonator with Fresnel number and with the fraction of the resonator filled by the oscillating line are in agreement with the data. It remains to change the geometric outcoupling of the resonator to see if the frequency of the oscillation will change as predicted.[1,2]

Table 10 Frequency and amplitude of time-dependent oscillations on individual lines for flow rates of run 34 at 5.3 Torr for scraper mirror slit widths of 3 mm and 4mm

Run 34, Symmetric confocal unstable resonator

Scraper mirror slit, mm	Lasing line	$P_1(4)$	$P_1(5)$	$P_1(6)$	$P_1(7)$	$P_1(8)$	$P_1(9)$	$P_2(5)$	$P_2(6)$	$P_2(7)$	$P_2(8)$
3.0	OSC period, ns			7 weak 40	40/7	7 weak 40	7		40/7	7 weak 40	7
	OSC freq., MHz			23-26	23-34	23-30			18-29	25-31	
	Amplitude Modulation $\%P_v(J)$				12.5				20-50	12	12.5
4.0	OSC period, ns										
	Data MNORO3UR[a]				40/7	40/7	weak 40		40	40/7	40/7
	5-mm slit	33	40	40	33			33	40-47	33-40	
	OSC Freq., MHz										
	Data MNORO3UR				20-30	20-30	20-30		20-28	18-30	22-30
	5-mm slit	30	25	25	30			30	21-25	25-30	
	Amplitude Modulation $\%P_v(J)$										
	Data MNORO3UR				38	80			20-30	66	55
	5-mm slit	82	100	76	18			83	92	40	

[a]Lines labeled MNORO3UR, 5-mm slit are results of calculation performed before the measurements were made to determine if time-dependent oscillations should occur when optical axis is 5 mm downstream of H_2 injectors.

V. Concluding Remarks

The Helios CL II stable resonator multiline performance with vacuum mirror mounts was measured as a function of the SF_6 and H_2 flow rates and mirror reflectivity. There was a distinct shift of the power spectral distribution toward higher J's as the flow rates increased and as the reflectivity increased. At the higher reflectivity, the additional lines $P_1(10)$, $P_1(12)$, and $P_2(10)$-$P_2(12)$ appeared with minima at $P_1(11)$ and $P_2(11)$. The occurrence of these lines is a result of the lower losses associated with the higher outcoupler reflectivity which permits lines with smaller gains to lase. The results of a stable resonator study indicated that the minima in the power spectral distribution at $P_1(11)$ and $P_2(11)$ are not a consequence of the type of resonator used. Thus, the minima at $P_1(11)$ and $P_2(11)$ may be evidence for a kinetic effect, namely, a near resonant energy transfer from $v=3$, $J=3,4$ to $v=2$, $J=14$, with a subsequent rotational cascade to $v=2$, $J=11$, which is the upper level for the $P_2(12)$ line. Since $P_2(12)$ lases, the rotational cascade to $v=2$, $J=10$, which is the upper level for the $P_2(11)$ line, is blocked, resulting in $P_2(11)$ being weaker than $P_2(12)$. A similar argument applies to the minimum at $P_1(11)$.

The saturation of the laser was varied by using externally mounted mirrors and Brewster windows. The cavity losses introduced by the Brewster windows were determined from the P_T vs reflectivity curves obtained from the vacuum mirror mount data. It was found that two Brewster windows have only slightly higher losses than one Brewster window. Rotation of the Brewster window showed that the losses were not affected by rotation of the polarization vector.

The performance of the laser with Brewster windows was measured as a function of the SF_6 and H_2 flow rates and effective reflectivity. There was a distinct shift of the power spectral distribution toward higher J's as the flow rates and the effective reflectivity increased. When a vacuum mirror mount case was compared to Brewster window cases of nearly equal effective reflectivities, a polarization effect was observed. At the higher SF_6 flow rates, the polarization promoted the appearance of $P_1(10)$ and $P_2(10)$-$P_2(12)$ with a minimum at $P_2(11)$. The minimum at $P_2(11)$ is not affected by the polarization but may be evidence for the kinetic effect described previously.

The model gave reasonable agreement with the data although it predicted more lines than are observed and the peak of the power spectral distributions is 1 or 2 J's too low. This is a consequence of the Fabry-Perot resonator employed in the calculations. When the calculations were repeated with a stable resonator model which includes the upstream-downstream coupling, better agreement with the data was achieved. The multiline output beam of the Helios CL II laser should be studied with a polarization analyzer to determine the direction of the polarization vector for the various optical configurations. To complement these experiments, the effects of polarization need to be incorporated into the computer models of the laser.

The amplitude, frequency, and Fresnel number dependence of the time-dependent oscillations which occur on lines whose saturated gain does not fill the unstable resonator were measured for the low SF_6 and H_2 flow rates. The good agreement with the data of the a priori prediction of these characteristics of the time-dependent oscillations by the MNORO3UR computer model provides confidence in the model's validity. Based on these results, the rotational nonequilibrium cw HF chemical laser models can be used with confidence in designing these devices. Finally, the geometric outcoupling of the unstable resonator should be varied to determine if the frequency of the time-dependent oscillations changes as predicted by the calculations.[1,2]

Acknowledgment

This study was supported by an AFSOR Grant.

References

[1]Sentman, L. H., "Chemical Laser Power Spectral Performance: A Coupled Fluid Dynamic, Kinetic and Physical Optics Model," *Applied Optics*, Vol. 17, July 1978, pp. 2244-2249.

[2]Sentman, L. H., Mosebach, W. O., and Renzoni, P., "A Theoretical and Experimental Study of cw Chemical Laser Performance," Aeronautical and Astronautical Engineering Dept., University of Illinois, Urbana, Ill., AAE 81-8, UILU Eng. 81-0508, Dec. 1981.

[3]Sentman, L. H., Schmidt, P. F., and Marinos, G. M., "Effects of the HF Rate Package and the Optical Resonator on cw HF Chemical Laser Performance," Aeronautical and Astronautical Engineering Dept., University of Illinois, Urbana, Ill., AAE 83-6, UILU Eng. 83-0506, June 1983.

[4]Turner, E. B., Chodzko, R. A., and Mirels, H., "Temporal Stability of Single Line cw HF Chemical Laser with Unstable Resonator," *Journal of Applied Physics*, Vol. 48, March 1977, p. 1163.

[5]Sentman, L. H. et al., "Theoretical and Experimental Study of cw HF Chemical Laser Performance," *Proceedings of the 4th International Symposium on Gas Flow and Chemical Lasers*, edited by M. Onorato, Plenum Publishing Corp., New York, 1984, pp. 173-182.

[6]Sentman, L. H., Subbiah, M., and Zelazny, S. W., "Blaze II, a Chemical Laser Simulation Program," Bell Aerospace Textron, Buffalo, N.Y., TR H-CR-77-8, 1977.

[7]Raymonda, J. W., Subbiah, M., Schimke, J. T., Zelazny, S. W., and Sentman, L. H., "Advanced HF and DF Chemical Laser Performance Modeling, Vol. I, The CNCDE/BLAZE Rotational Equilibrium Code," Bell Aerospace Textron, Buffalo, N.Y., TR DRCPM-HEL-CR-79-7, 1979.

[8]Sentman, L. H. and Rushmore, W., "Computationally Efficient Rotational Nonequilibrium cw Chemical Laser Model," *AIAA Journal*, Vol. 19, Oct. 1981, pp. 1323-1332.

[9]Sentman, L. H. and Schmidt, P., "MNORO3: An Efficient Rotational Nonequilibrium cw HF Chemical Laser Model," Aeronautical and Astronautical Engineering Dept., University of Illinois, Urbana, Ill., TR AAE 83-1, UILU Eng. 83-0501, Jan. 1983.

[10]Townsend, S. W. and Sentman, L. H., "Design of a Constant Efficiency Spectrometer for IR Wavelengths," *Applied Optics*, Vol. 23, July 15, 1984, pp. 2393-2400.